A&A 516, A84 (2010)
DOI: 10.1051/0004-6361/200913874

Astronomy & Astrophysics

Instability of twisted magnetic tubes with axial mass flows

T. V. Zaqarashvili[1,3], A. J. Díaz[2], R. Oliver[2], and J. L. Ballester[2]

[1] Space Research Institute, Austrian Academy of Sciences, Graz, Austria
e-mail: teimuraz.zaqarashvili@oeaw.ac.at
[2] Departament de Física, Universitat de les Illes Balears, 07122 Palma de Mallorca, Spain
e-mail: [toni.diaz;ramon.oliver;dfsjlb0]@uib.es
[3] Abastumani Astrophysical Observatory at Ilia State University, Kazbegi ave. 2a, Tbilisi, Georgia

Received 15 December 2009 / Accepted 16 March 2010

ABSTRACT

Context. Recent observations of various kinds of jets in the solar atmosphere motivate studying the influence of mass flow on the stability of solar magnetic structures.
Aims. We study the influence of axial mass flows on the stability of twisted magnetic flux tubes.
Methods. We use the incompressible magnetohydrodynamic equations to get the dispersion relation governing the behaviour of normal modes in uniformly twisted magnetic tubes with sub-Alfvénic flows. The dispersion relation is then solved analytically and numerically to find stability criteria for twisted tubes with flow.
Results. Two main important results are found. First, the axial mass flow reduces the threshold of kink instability in twisted magnetic tubes. Second, the twist of magnetic tubes leads to the Kelvin-Helmholtz instability of sub-Alfvénic flows for the harmonics with a large enough azimuthal wave number $-m$.
Conclusions. The observed mass flow may trigger the kink instability in magnetic configurations that are near their stability threshold, leading to solar flares and coronal mass ejections. The effect is more significant for photospheric magnetic tubes than for coronal ones. Sub-Alfvénic flows undergo the Kelvin-Helmholtz instability in slightly twisted magnetic tubes if the azimuthal wavenumber is big enough.

Key words. magnetohydrodynamics (MHD) – instabilities – Sun: atmosphere

1. Introduction

Recent observations with high spatial and temporal resolutions have revealed the complex structure and dynamics of the solar atmosphere. Various jets and flows are observed in photospheric/chromospheric magnetic structures (Katsukawa et al. 2007; Shibata et al. 2007; De Pontieu et al. 2007; Nishizuka et al. 2008), coronal loops (Shibata et al. 1992; Winebarger et al. 2002; Ofman & Wang 2008), prominences (Lin et al. 2003, 2005; Okamoto et al. 2007) and coronal holes (Cirtain et al. 2007; Scullion et al. 2009).

Hydrodynamic flows are generally subject to the classical Kelvin-Helmholtz instability (Drazin & Reid 1981). A flow-aligned magnetic field may stabilise sub-Alfvénic flows, while a transverse magnetic field seems to have no effect on the instability (Chandrasekhar 1961; Sen 1963; Ferrari et al. 1981; Cohn 1983). Therefore, the magnetic field topology is crucial for the threshold of flow instability; namely, the twist of magnetic tubes may affect the instability properties of axial mass flows.

Oscillations of magnetic tubes with mass flows have been studied intensively (Roberts 1987; Goossens et al. 1992; Terra-Homem et al. 2003; Soler et al. 2008, 2009, 2010; Gruszecki et al. 2008; Terradas et al. 2008, 2010; Vasheghani Farahani et al. 2009). They show that including flow modifies the phase speeds and consequently the propagation properties of tube waves. However, all these works consider the effect of mass flow on the magnetohydrodynamic oscillations of untwisted magnetic tubes. The considered flows are essentially sub-Alfvénic, hence below the threshold of the Kelvin-Helmholtz instability.

The solar magnetic field has quite complicated topology in the whole solar atmosphere. Photospheric motions may stretch and twist anchored magnetic fields, which may lead to the consequent changes in topology at higher regions. The observed rotation of sunspots (Brown et al. 2003; Yan & Qu 2007) may lead to twisting of the magnetic tubes above active regions. On the other hand, the newly emerged magnetic tubes are supposed to be twisted during the rising phase through the convection zone (Moreno-Insertis & Emonet 1996; Archontis et al. 2004; Murray & Hood 2008; Hood et al. 2009). Therefore, solar magnetic tubes should have been twisted at photospheric, chromospheric, and coronal levels. Solar prominences are also supposed to be formed in a twisted magnetic field (Priest et al. 1989). However, not all works on prominence formation and equilibrium assume twisted fields, and the issue is still not clear today.

Magnetic tubes are subject to the kink instability when the twist exceeds a critical value (Lundquist 1951; Hood & Priest 1979). The kink instability may then be the triggering mechanism for solar flares, which may heat the coronal plasma (Velli et al. 1990; Linton et al. 1998; Gerrard et al. 2004; Browning et al. 2008), and for filament instabilities, which may lead to coronal mass ejections (CMEs) (Zhou et al. 2006; Liu et al. 2007).

The normal mode analysis of twisted magnetic tubes without flow has been performed in early works (Dungey & Loughhead 1954; Roberts 1956; Bennett et al. 1999; Carter & Erdélyi 2008), and they show a threshold of the kink instability similar to what is obtained by an energy consideration method (Lundquist 1951). However, a flow along the twisted magnetic

tube may decrease the threshold for the kink instability, as recently supposed and tested experimentally (Furno et al. 2007). Then, the observed flows may trigger solar flares and CMEs, which may have a tremendous importance for solar physics and space weather predictions.

In this paper, we aim to study the stability of twisted magnetic tubes with axial mass flows using normal mode analysis. We consider two different phenomena. First, we show that the threshold of kink instability is decreased due to the mass flow. And second, the Kelvin-Helmholtz instability may take place for sub-Alfvénic flows because of the twist of magnetic tubes.

2. Formulation of the problem and dispersion relation

We consider a magnetic flux tube with density ρ_0 embedded in a field-free environment with density ρ_e. Both ρ_0 and ρ_e are supposed to be homogeneous. The cylindrical coordinate system (r, ϕ, z) is used, where the magnetic field has the following form: $(0, B_\phi(r), B_z(r))$. The unperturbed magnetic field and pressure satisfy the pressure balance condition

$$\frac{\mathrm{d}}{\mathrm{d}r}\left(p + \frac{B_\phi^2 + B_z^2}{8\pi}\right) = -\frac{B_\phi^2}{4\pi r}. \tag{1}$$

We consider the mass flow $(0, 0, U_z)$ inside the magnetic tube directed along the z axis, so the equilibrium mass flow is not field-aligned. Magnetic field lines are just being dragged by the flow without deformation, so no electric currents arise during the motion. Boundary conditions in the longitudinal direction may create some problems, but not in our case of an unbounded tube. In general, U_z can be a function of r, but we consider the simplest homogeneous case. No mass flow is considered outside the tube, so the surrounding coronal medium is considered to be unmagnetised ($B_{\mathrm{ext}} = 0$), uniform (ρ_e constant), and lacking mass flow at the equilibrium.

As the unperturbed parameters only depend on the r coordinate, the perturbations can be Fourier-analysed with $\exp[\mathrm{i}(m\phi + kz - \omega t)]$. The equations governing the incompressible dynamics of the plasma are (Goossens et al. 1992)

$$D\frac{\mathrm{d}}{\mathrm{d}r}(r\xi_\mathrm{r}) = C_1 r\xi_\mathrm{r} - C_2 r p_\mathrm{t}, \tag{2}$$

$$D\frac{\mathrm{d}p_\mathrm{t}}{\mathrm{d}r} = C_3\xi_\mathrm{r} - C_1 p_\mathrm{t}, \tag{3}$$

where

$$D = \rho\left(\Omega^2 - \omega_\mathrm{A}^2\right),\ C_1 = -\frac{2mB_\phi}{4\pi r^2}\left(\frac{m}{r}B_\phi + kB_z\right),$$
$$C_2 = -\left(\frac{m^2}{r^2} + k^2\right),\ C_3 = D^2 + D\frac{2B_\phi}{4\pi}\frac{\mathrm{d}}{\mathrm{d}r}\left(\frac{B_\phi}{r}\right) - \frac{4B_\phi^2}{4\pi r^2}\rho\omega_\mathrm{A}^2,$$

$$\omega_\mathrm{A} = \frac{1}{\sqrt{4\pi\rho}}\left(\frac{m}{r}B_\phi + kB_z\right), \tag{4}$$

and

$$\Omega = \omega - kU_z \tag{5}$$

is the Doppler-shifted frequency.

Here ξ_r is the radial displacement and p_t the total (hydrostatic+magnetic) perturbed pressure. Equations (2), (3) can be cast into one equation:

$$\frac{\mathrm{d}^2 p_\mathrm{t}}{\mathrm{d}r^2} + \left[\frac{C_3}{rD}\frac{\mathrm{d}}{\mathrm{d}r}\left(\frac{rD}{C_3}\right)\right]\frac{\mathrm{d}p_\mathrm{t}}{\mathrm{d}r} + \left[\frac{C_3}{rD}\frac{\mathrm{d}}{\mathrm{d}r}\left(\frac{rC_1}{C_3}\right) + \frac{C_2C_3 - C_1^2}{D^2}\right]p_\mathrm{t} = 0. \tag{6}$$

The solution of this equation depends on the magnetic field and density profiles. We consider a magnetic flux tube with homogeneous density ρ_0 and uniform twist, i.e. $(0, Ar, B_0)$, with A a constant; we define $c_{\mathrm{A}0} = B_0/\sqrt{4\pi\rho_0}$. In this case Eq. (6) reduces to the modified Bessel equation

$$\frac{\mathrm{d}^2 p_\mathrm{t}}{\mathrm{d}r^2} + \frac{1}{r}\frac{\mathrm{d}p_\mathrm{t}}{\mathrm{d}r} - \left[\frac{m^2}{r^2} + m_0^2\right]p_\mathrm{t} = 0, \tag{7}$$

where

$$m_0^2 = k^2\left[1 - \frac{4A^2\omega_\mathrm{A}^2}{4\pi\rho_0\left(\Omega^2 - \omega_\mathrm{A}^2\right)^2}\right]. \tag{8}$$

A similar equation has been obtained by Dungey & Loughhead (1954) and Bennett et al. (1999) in the absence of flow, i.e. for $U_z = 0$.

The solution bounded at the tube axis is

$$p_\mathrm{t} = a_0 I_\mathrm{m}(m_0 r), \tag{9}$$

where I_m is the modified Bessel function of order m.

The total pressure perturbation outside the tube is governed by the same Bessel equation, but m_0^2 is replaced by k^2. The solution bounded at infinity is

$$p_\mathrm{t} = a_\mathrm{e} K_\mathrm{m}(kr). \tag{10}$$

In the following we always consider positive k. The boundary conditions at the tube surface $r = a$ are the continuity of Lagrangian displacement and total Lagrangian pressure (Dungey & Loughhead 1954; Roberts 1956; Bennett et al. 1999), i.e.,

$$[\xi_\mathrm{r}]_a = 0 \tag{11}$$

and

$$\left[p_\mathrm{t} - \frac{B_\phi^2}{4\pi a}\xi_\mathrm{r}\right]_a = 0. \tag{12}$$

Using these conditions we can derive the dispersion equation governing the oscillations of a twisted magnetic tube with axial mass flow

$$\frac{\left[(\tilde{\omega} - kpM_\mathrm{A})^2 - (m + kp)^2\right]F_\mathrm{m}(m_0 a) - 2m(m + kp)}{[(\tilde{\omega} - kpM_\mathrm{A})^2 - (m + kp)^2]^2 - 4(m + kp)^2} = \frac{P_\mathrm{m}(ka)}{\tilde{\omega}^2\rho_\mathrm{e}/\rho_0 + P_\mathrm{m}(ka)}, \tag{13}$$

where

$$F_\mathrm{m}(m_0 a) = \frac{m_0 a I'_\mathrm{m}(m_0 a)}{I_\mathrm{m}(m_0 a)},\quad P_\mathrm{m}(ka) = \frac{kaK'_\mathrm{m}(ka)}{K_\mathrm{m}(ka)}, \tag{14}$$

$$M_\mathrm{A} = \frac{\sqrt{4\pi\rho_0}U_z}{B_0} = \frac{U_z}{c_{\mathrm{A}0}},\ p = \frac{B_0}{A},$$

$$m_0^2 = k^2\left[1 - \frac{4(m+kp)^2}{[(\tilde{\omega} - kpM_A)^2 - (m+kp)^2]^2}\right]. \quad (15)$$

Here M_A is the Alfvén Mach number, $2\pi p$ the pitch, and $\tilde{\omega}$ the normalised frequency $\tilde{\omega} = \omega\sqrt{4\pi\rho_0}/A = \omega\, kp/(c_{A0}k)$. The pitch is the longitudinal distance between neighbouring turns of magnetic field in twisted tubes, and it can be also expressed as the ratio of the tube length to the number of turns along the whole tube. The dispersion relation is the generalisation of that of Dungey & Loughhead (1954) and Bennett et al. (1999), incorporating the flow effects (new additional terms containing M_A). Considerating $M_A = 0$ in Eq. (13) leads to the dispersion relation (24) of Dungey & Loughhead (1954). There is a typographical sign error in their dispersion relation as noticed by Bennett et al. (1999). The sign of m_0^2 defines the type of tube waves: $m_0^2 > 0$ corresponds to surface waves and $m_0^2 < 0$ corresponds to body waves, which have an ordinary Bessel function in the radial dependence instead of Eq. (9) so the Bessel function $I_m(m_0a)$ is replaced by $J_m(m_0a)$ in Eq. (14).

Complex solutions of the dispersion relation (Eq. (13)) indicate the instability conditions of the twisted magnetic tube with mass flow, since one of the solutions has a positive imaginary part and grows exponentially in time. We first concentrate on the instability of the $m = 1$ kink mode and then turn to the Kelvin-Helmholtz instability of sub-Alfvénic flows.

3. Kink instability of a twisted tube with a mass flow

The threshold for the kink instability can be found analytically through the marginal stability analysis, i.e. considering $\omega = 0$ (Chandrasekhar 1961; Dungey & Loughhead 1954; Bennett et al. 1999). However, in our case the marginal stability should be derived by setting $\Omega = 0$ or $\tilde{\omega} = kpM_A$. This is clearly seen in Figs. 1 and 2, where the numerical solutions of the dispersion relation (13) are presented for tubes with photospheric and coronal conditions, respectively. The figures show the real and imaginary parts of frequency versus the wave number ka in non-flow $M_A = 0$ (top panel) and flow $M_A = 0.75$ (bottom panel) regimes for $m = 1$ kink mode. There are many stable harmonics represented by solid lines in the upper parts of the plots, which merge towards the frequency for which the denominator in Eq. (15) vanishes, namely,

$$\tilde{\omega}_{band} = \pm(m + kp) + kpM_A. \quad (16)$$

This equation is obtained when $\Omega = \pm\omega_A$ i.e. when the Doppler-shifted frequency equals the Alfvén frequency. This so-called Alfvén resonance determines the frequency, for which resonant absorption may take place in inhomogeneous plasmas. However, in our case, ω_A is constant and this avoids further complications. In the lower part of the plots we see harmonics whose frequencies tend to zero for increased ka if $M_A = 0$ or that merge with other modes if $M_A \neq 0$. These are bifurcations that correspond to the instability threshold. In the non-flow $M_A = 0$ case the bifurcation occurs when $\tilde{\omega}$ is zero, while for $M_A = 0.75$ the bifurcation begins for $\Omega \approx 0$ or $\tilde{\omega} \approx kpM_A$. For higher values of kp, other modes might become unstable, too.

Therefore, we study the marginal stability by adopting $\tilde{\omega} = kpM_A$ in the dispersion relation (Eq. (13)), which takes the form

$$F_m(m_0a) = -\frac{P_m(ka)[(m+kp)^2 - 4]}{k^2p^2M_A^2\rho_e/\rho_0 + P_m(ka)} - \frac{2m}{m+kp}, \quad (17)$$

where

$$m_0^2 = k^2\left[1 - \frac{4}{(m+kp)^2}\right]. \quad (18)$$

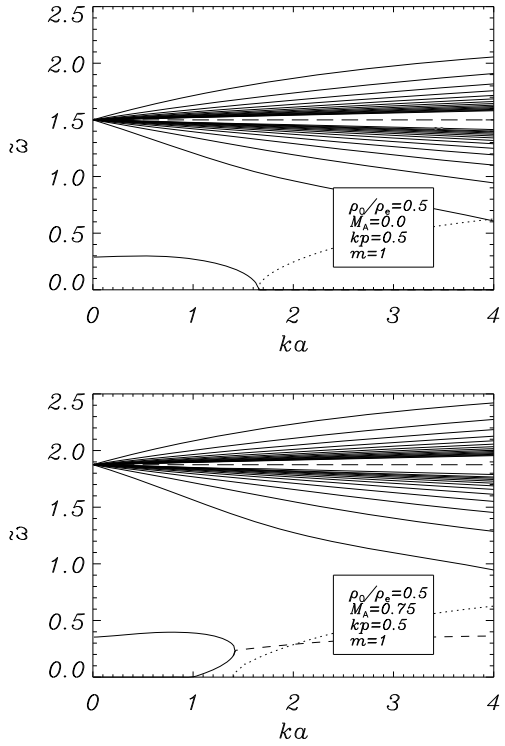

Fig. 1. Frequency versus wave number calculated from the dispersion relation (Eq. (13)) for the kink mode ($m = 1$) and a density ratio typical of photospheric conditions, $\rho_0/\rho_e = 0.5$. Solid lines represent the real frequency (stable regime), while dashed and dotted lines represent the real and imaginary parts of the complex frequency (unstable regime). Top and bottom panels show the solutions without ($M_A = 0.0$) and with ($M_A = 0.75$) flow. Higher stable overtones converge to the kink frequency when ka tends to 0. The unstable mode is seen in the lower left corners of both plots as a bifurcation. In the case $M_A = 0$ the mode becomes unstable at $ka \approx 1.65$, while in the case $M_A = 0.75$ the instability begins at $ka \approx 1.4$. Only the 15 modes further from the accumulation band are shown in this plot, while the long-dashed line is the central frequency of this band (Eq. (16)).

Then, following the calculations of Dungey & Loughhead (1954) and Bennett et al. (1999), if $(m + kp)^2 > 4$, then m_0 is real and we can observe that

$$\frac{m_0aI_m'(m_0a)}{I_m(m_0a)} > |m|. \quad (19)$$

The right-hand side of Eq. (17) is smaller than $|m|$, so this equation is not satisfied in the above conditions. If $(m + kp)^2 = 4$, then $m_0 = 0$ and the boundary conditions are not satisfied (see Dungey & Loughhead 1954). Therefore, the condition for marginal instability is

$$(m + kp)^2 < 4. \quad (20)$$

In this situation it is convenient to use

$$n_0^2 = -m_0^2 = k^2\left[\frac{4}{(m+kp)^2} - 1\right]. \quad (21)$$

We can derive the stability condition for each mode with different m. Equation (20) shows that only the $m < 2$ modes can be unstable when m and kp have the same sign. However, higher order harmonics can also be unstable if m and kp have different signs (see the next section). Let us now discuss the kink $m = 1$ mode.

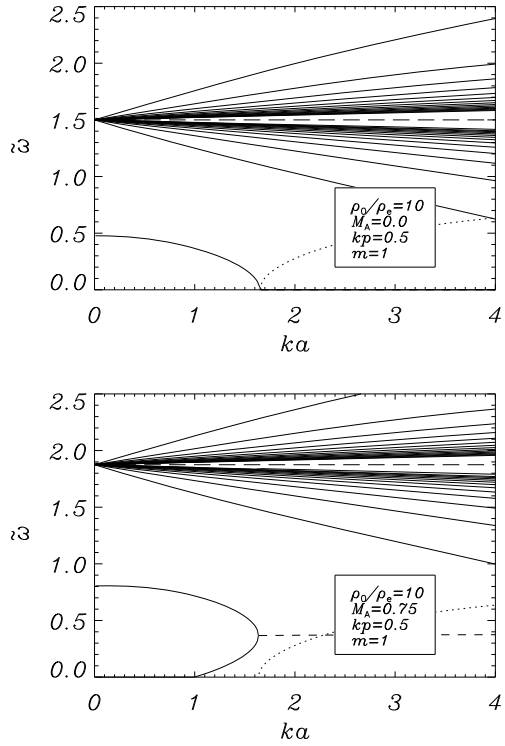

Fig. 2. Same as Fig. 1 for a density ratio typical of coronal conditions, $\rho_0/\rho_e = 10$.

For the kink mode, Eq. (17) is rewritten as

$$F_1(m_0 a) = -\frac{P_1(ka)[(1+kp)^2-4]}{k^2p^2M_A^2\rho_e/\rho_0 + P_1(ka)} - \frac{2}{1+kp}. \quad (22)$$

The long wavelength approximation $(ka)^2 \ll 1$ gives

$$\frac{n_0 a J_1'(n_0 a)}{J_1(n_0 a)} \approx 1 - \frac{1}{4}(n_0 a)^2 + ...$$

and $P_1 \approx -1$. Then, from Eq. (22) we get the instability criterion for small kp and ka as

$$a > 2p\,(1+kp)\,\sqrt{1 - M_A^2\rho_e/\rho_0}. \quad (23)$$

This is Eq. (38) of Bennett et al. (1999) multiplied by $\sqrt{1 - M_A^2\rho_e/\rho_0}$. Equation (23) shows that the axial flow reduces the threshold of the kink instability in twisted tubes (see similar conclusion in a very simplified case by Furno et al. 2007). The Kruskal-Shafranov instability criterion yields $\Phi = LB_\phi/aB_z > 2\pi$, where Φ is the total twist angle of magnetic tube with the length L and the radius a, and hence $B_\phi/B_z > 2\pi a/L$. Line tying of tube ends generally increases the critical twist angle, and the instability threshold becomes $\Phi > 2.5\pi$ (Hood & Priest 1979). However, for a high aspect ratio (i.e. the ratio of the loop length to the radius), the critical twist angle increases further (Baty 2001). Here we consider unbounded magnetic tubes, therefore the comparison of our results with Kruskal-Shafranov criterion is not straightforward. However, for the long wave length approximation (or high aspect ratio) Eq. (23) can be rewritten as $B_\phi/B_z > 2\sqrt{1 - M_A^2\rho_e/\rho_0}$. Thus, thin and long tubes yield a larger critical twist angle as shown by Baty (2001). Recent observations of kink instability in a coronal loop during a small B5.0 solar flare show a large twist angle of 12π, which confirms the increase of critical twist for coronal loops with a high aspect ratio (Srivastava et al. 2010). The longitudinal flow may reduce the critical angle. For example, a flow of 0.75 V_A may reduce the twist angle in photospheric ($\rho_e \sim \rho_0$) and coronal ($\rho_0 \sim 2\rho_e$) tubes by 60% and 20%, respectively.

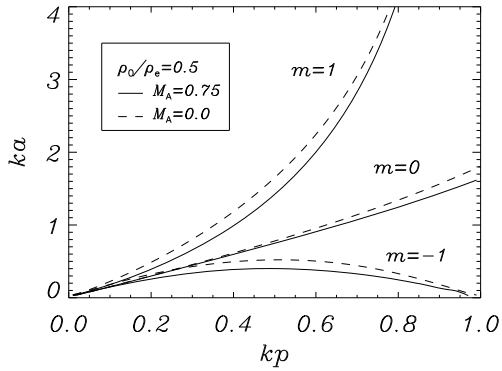

Fig. 3. Stability diagram of the $m = 0, \pm 1$ modes in the presence of axial mass flow (solid lines). The dashed lines represent the solutions without flow (Dungey & Loughhead 1954). Equilibrium configurations whose parameters are above the stability lines are unstable. It is clearly seen that the flow reduces the thresholds of instabilities.

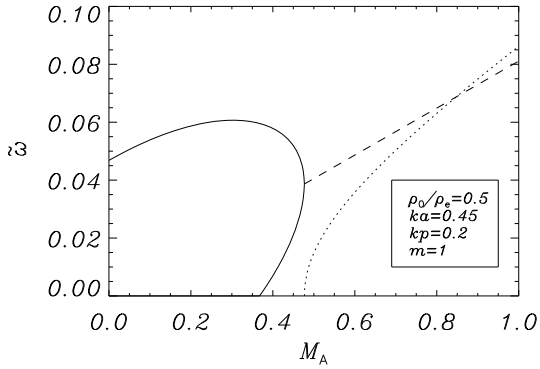

Fig. 4. Dependence on the flow speed of the instability threshold of the particular $m = 1$ harmonic with $ka = 0.45$ and $kp = 0.2$. The solid line represents the real frequency, while the dashed (dotted) line corresponds to the real (imaginary) part of the complex frequency. The frequency becomes complex when the flow speed reaches about 0.45 the Alfvén speed.

Complex solutions at the bifurcation points are also shown in Fig. 1. It is clearly seen how the stable regime is replaced by the unstable one when increasing ka. The instability begins for smaller ka in the presence of flow (bottom panel), and the real part of the unstable mode is zero in the case $M = 0$.

Figure 3 shows an stability diagram similar to those of Dungey & Loughhead (1954) and Bennett et al. (1999) incorporating the mass flow effects for a photospheric density ratio. The equivalent plots of the non-flow solution of Dungey & Loughhead (1954) have been overplotted for better comparison. Including the flow shifts the stability curve down, thus making the configuration more unstable, but we can check that even for such a high Alfvén Mach number the shift is relatively small.

The dependence of the instability threshold on the flow is clearly seen in Fig. 4, where the frequency dependence of the particular $m = 1$ harmonic with $ka = 0.45$ and $kp = 0.2$ on the flow speed is shown (both real and imaginary parts). We see that the harmonic is stable for $M_A = 0$ and becomes unstable for $M_A \approx 0.45$. The same relation can be derived from the analytical stability criterion (23). This clearly shows the destabilising

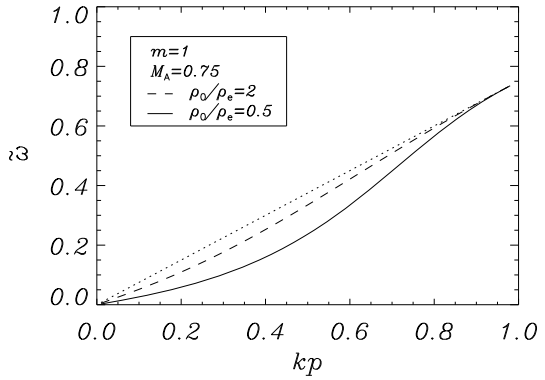

Fig. 5. Real part of the frequency at the bifurcation point. The dotted line is $\Omega = 0$ ($\tilde{\omega} = kpM_A$), while the dashed and solid lines correspond to coronal ($\rho_e < \rho_0$) and photospheric ($\rho_e > \rho_0$) tubes with flow speed $U_z = 0.75c_{A0}$. We can see that $\Omega = 0$ is a much better approximation than $\tilde{\omega} = 0$, specially under coronal conditions.

effect of the flow, since a mode that is stable (although close to the instability margin), becomes unstable when the flow speed is increased.

Equation (23) shows that the flow effect is more efficient for magnetic tubes with $\rho_e > \rho_0$ (photospheric tubes, coronal holes) than for dense ones, with $\rho_e < \rho_0$ (coronal loops), since the term $\tilde{\omega}^2\rho_e/\rho_0$ is much smaller than $P_m(ka)$ in the right-hand side of Eq. (13) when the frequency is close to the stability threshold. In that condition, we can consider that Eq. (13) is approximately equal to the dispersion relation found in Dungey & Loughhead (1954) and Bennett et al. (1999) when substituting their frequency by the Doppler-shifted frequency Ω (Eq. (5)). Therefore, the stability diagrams are very close to the $M_A = 0$ counterparts in coronal conditions (and even closer in prominence conditions, since $\rho_e \ll \rho_0$). Figure 5 shows the dependence of the stability threshold on the density ratio for less dense tubes, which correspond to the photosphere and coronal holes, and for dense coronal loops. Indeed, the photospheric tubes are more sensitive to the axial flows than the coronal ones, since the threshold is further from the Doppler-shifted frequency Ω, caused by the right-hand side of Eq. (13) being further from unity and the only non-Doppler-shifted frequency term in Eq. (13) being relevant. Even in the photospheric case, the frequency of the stability threshold is still close to Ω, thus justifying the assumption made to obtain Eq. (17).

The numerical solutions of the dispersion relation (Eq. (13)) confirm the validity of the analytical stability criterion (23). It is seen that the axial flow reduces the threshold of the kink instability. The twisted magnetic tube, which is stable in the absence of flow, thus becomes unstable when plasma begins to flow along its axis. Therefore, the plasma flow may trigger the kink instability in otherwise stable magnetic configurations in our model, but for typical values in the solar atmosphere, the configuration without flow must be close to the stability threshold for the twist to become unstable when the flow is added. For less twisted tubes, the addition of flow does not induce the kink instability even for high values of the Alfvén Mach number.

4. Kelvin-Helmholtz instability of sub-Alfvénic flows in twisted magnetic tubes

The Kelvin-Helmholtz instability of inhomogeneous flows is a hydrodynamic phenomenon that is eventually suppressed by including a sufficiently large flow-aligned magnetic field. It is generally believed that sub-Alfvénic, field-aligned flows are stable. However, the perpendicular component of the magnetic field seems to have no effect on the instability (Chandrasekhar 1961; Sen 1963; Ferrari et al. 1981; Cohn 1983; Singh & Talwar 1994). Then, a flow with an angle to the magnetic field always has a component perpendicular to the field, which can be unstable. Therefore, the flow along the twisted tube should be unstable even if its speed is less than Alfvénic. In this section, we show that this indeed happens in our model.

We consider perturbations propagating nearly perpendicular to the magnetic field, which seem to be most unstable ones (Pataraya & Zaqarashvili 1995). For these perturbations $\boldsymbol{k} \cdot \boldsymbol{B} \approx 0$, and since in this paper $\boldsymbol{k} \approx (m_0, m, k)$ in cylindrical coordinates, this condition gives

$$m \approx -kp \tag{24}$$

using the definition of the pitch in Eq. (14).

Then, Eq. (13) is significantly simplified to the expression:

$$\left[F_m(ka)\,\rho_e/\rho_0 - P_m(ka)\right]\tilde{\omega}^2 + 2kpM_A P_m(ka)\tilde{\omega} + P_m(ka)\left[F_m(ka) - k^2p^2M_A^2\right] = 0. \tag{25}$$

Using the long wave length approximation, $ka \ll 1$, we have

$$F_m(ka) = \frac{kaI_m'(ka)}{I_m(ka)} \approx |m|$$

and

$$P_m(ka) = \frac{kaK_m'(ka)}{K_m(ka)} \approx -|m|,$$

which gives

$$(1 + \rho_e/\rho_0)\,\tilde{\omega}^2 - 2kpM_A\tilde{\omega} + k^2p^2M_A^2 - |m| = 0. \tag{26}$$

The solution of this algebraic equation using the approximation of Eq. (24) is

$$\tilde{\omega}_\pm = \frac{|m|}{1 + \rho_e/\rho_0}\left(-M_A \pm \sqrt{1 + \rho_e/\rho_0 - |m|M_A^2\rho_e/\rho_0}\right). \tag{27}$$

The condition for $\tilde{\omega}$ to be complex is

$$|m|M_A^2 > 1 + \rho_0/\rho_e. \tag{28}$$

Thus, the harmonics with sufficiently high m are unstable for any value of M_A. Equation (28) is the criterion for the Kelvin-Helmholtz instability of sub-Alfvénic flows in twisted magnetic tubes for our particular choice of the equilibrium magnetic field.

Figure 6 displays the numerical solution of the dispersion relation in Eq. (13) for a magnetic tube with $\rho_e/\rho_0 = 2$ and $M_A = 0.75$, corresponding to the flow speed $U_z = 0.75c_{A0}$. For this case, the instability criterion of Eq. (28) yields the critical value $m = 2.66$. Indeed, we see in the figure that the $m = 2$ modes (top panel) are always stable, while some $m = 3$ modes have complex frequencies so are unstable in the wave number interval around $kp = -3$, as suggested by Eq. (24). The modes located in the interval $-4 < kp < -2.5$ are unstable, therefore Eq. (24) is not a strict criterion. Modes that propagate nearly perpendicular to the magnetic field are all unstable, therefore the instability develops very quickly, even if kp is not exactly $-m$ (and the propagation is not purely perpendicular to the field).

Figure 7 shows the transition from stable to unstable regimes for $m = 6$ modes near the critical flow speed value $U_z = 0.5c_{A0}$ ($M_A = 0.5$), which is estimated from Eq. (28). We see the two

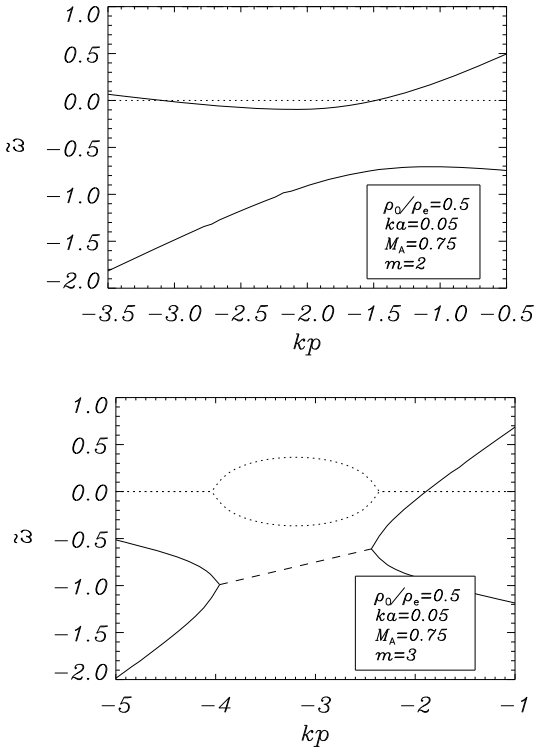

Fig. 6. Frequency versus kp for $m = 2$ and $m = 3$ modes when the flow speed is $U_z = 0.75c_{A0}$. Solid and dashed lines are the real part of the frequency of stable and unstable modes, respectively, while dotted lines are the imaginary part of the frequency.

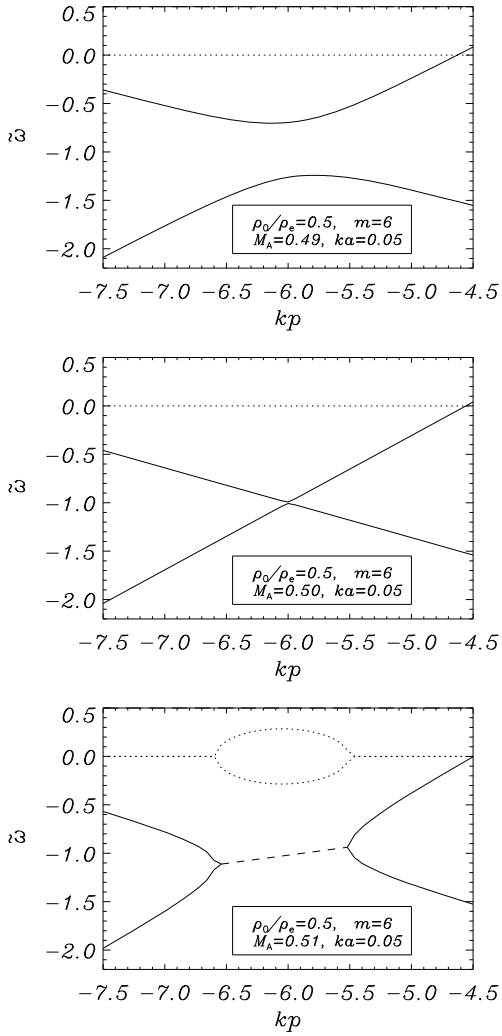

Fig. 7. Frequency versus kp for $m = 6$ modes for three different values of the flow speed. The two modes are stable for $U_z = 0.49c_{A0}$ (*top panel*), they come very close near $kp = -6$ for $U_z = 0.5c_{A0}$ but still remain stable (*middle panel*), and they become unstable for $U_z = 0.51c_{A0}$ (*bottom panel*). Line styles are as in Fig. 6.

stable modes for $M_A = 0.49$ (top panel), then the modes become very close for $M_A = 0.5$, but still stay stable (middle panel), and they finally become unstable for $M_A = 0.51$ (bottom panel). Again, the instability occurs inside the whole interval $-6.5 < kp < -5.5$. We can check Eq. (28) from a different point of view by plotting the frequency of the solutions for a fixed value of the flow speed for different values of the azimuthal number, which is plotted in Fig. 8. For the parameters used here, the threshold value is $m = 6$, and the instability is triggered for higher values of m.

Numerical solutions of the dispersion relation Eq. (13) show that many modes propagating with an angle to the normal of the unperturbed magnetic field are unstable. Therefore, sub-Alfvénic flows in slightly twisted magnetic tubes quickly become unstable owing to the Kelvin-Helmholtz instability.

Equation (28) is derived for the long wavelength approximation, but it is interesting to show the growth rates for the modes with different wavelengths. Figure 9 shows the dependence of real and imaginary parts of frequency on ka for $\rho_e/\rho_0 = 0.5$, $m = 3$, $M_A = 0.75$, and $kp = -3.6$ (inside the instability region in Fig. 6). The bifurcations above the upper frequency band are due to the Kelvin-Helmholtz instability. The growth rate is stronger for smaller ka, making the modes with longer wave length the most unstable. However, there are unstable modes with shorter wave lengths as well. It is difficult to judge the penetration depth of the instability into magnetic tubes in the framework of linear theory. However, some estimations can be made using the solution inside the tube, e.g., Eq. (9). The unstable modes with smaller ka and larger m are probably located near the tube surface, while the modes with larger ka may penetrate deeper and cause the destabilisation of the whole tube. Intense numerical simulations are needed for a detailed study of this problem.

5. Discussion

Axial mass flows and twisting of magnetic flux tubes lead to two different instability processes, which are well studied separately in previous works. Axial flows in untwisted magnetic tubes may lead to the Kelvin-Helmholtz instability, which is essentially a hydrodynamic phenomenon. A sufficiently strong magnetic field (with $M_A \geq 1$) completely stabilises the instability (Chandrasekhar 1961; Sen 1963; Ferrari et al. 1981; Cohn 1983). On the other hand, twisted magnetic tubes without flow may undergo the kink instability when the twist exceeds a critical value with the stability criterion $2p < a$ (Lundquist 1951). We have shown that the joint action of axial mass flow and twisting increases the probability of instability in magnetic tubes. Both kink and Kelvin-Helmholtz instabilities require separate discussions.

The kink instability is connected to the symmetric ($m = 1$) mode, which displaces the tube axis. When the tube is twisted, then the displacement of the axis leads to inhomogeneous twists

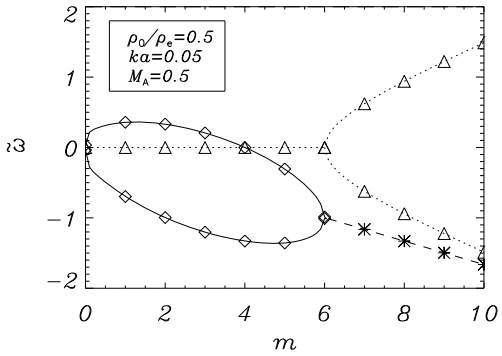

Fig. 8. Frequency versus m for a fixed value of the flow speed. Here we solved Eq. (13) considering $m = -kp$ as a real number, but the symbols mark the positions were m is an integer, hence a physically meaningful solution. Solid lines correspond to real solutions and the dashed line to the real part of imaginary solutions, while dotted lines represent the imaginary part of the solutions.

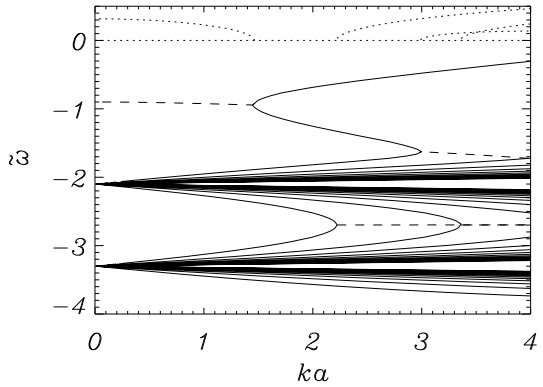

Fig. 9. Frequency versus wave number calculated from the dispersion relation (Eq. (13)) for the parameters $m = 3$, $\rho_0/\rho_e = 0.5$, $M_A = 0.75$ and $kp = -3.6$. Solid lines represent the real frequency (stable modes), while dashed and dotted lines represent the real and imaginary parts of the complex frequency, respectively (unstable modes). Here negative values have also been plotted, so both accumulation bands are shown, and only the 15 modes further from each accumulation band are included in this plot.

on opposite sides of the displacement, which eventually causes the instability. It turns out that the axial mass flow decreases the threshold for the instability; i.e. the instability may set on with smaller twist. Therefore, if the magnetic configuration is in a stable static equilibrium, then the mass flow may lead to its destabilisation. The phenomenon is more pronounced in photospheric magnetic tubes, i.e., when $\rho_0 < \rho_e$. Dense coronal loops and prominence threads with $\rho_0 > \rho_e$ are less affected by the flow. However, if the configurations are near the threshold, then even sub-Alfvénic flows may trigger the kink instability, which then may lead to solar flares and CMEs, Therefore, flows can be important in coronal loops and prominence plasma as well.

The Kelvin-Helmholtz instability is essentially a flow-induced phenomenon and is strongly affected by the axial magnetic field. However, even a slight twist of the magnetic tube leads to the instability of sub-Alfvénic flows. In this case, the flow vector has a component perpendicular to the magnetic field, which behaves as a hydrodynamic flow undergoing the Kelvin-Helmholtz instability. We have shown that unstable modes propagate nearly perpendicular to the magnetic field, i.e., $\boldsymbol{k} \cdot \boldsymbol{B} \approx 0$, which in our notations gives $m \approx -kp$. Therefore, any sub-Alfvénic mass motion can be unstable if it flows along twisted magnetic tubes. This phenomenon can be important for recently observed numerous jets and motions in the solar atmosphere. For example, the type II spicules, observed in the solar chromosphere by SOT (solar optical telescope) on board the Hinode spacecraft, have high upward flow speeds (but probably still sub-Alfvénic) of 50–150 km s^{-1} and short life times of 10–150 s (De Pontieu et al. 2007). The short life time of these features has not been explained yet; however, they can undergo the Kelvin-Helmholtz instability and fade away rapidly if they flow along twisted magnetic fields. This suggestion can be tested by observations.

It must be mentioned that here we consider the simplest incompressible approximation (infinite sound speed). This is because of mathematical difficulties associated to twisted configurations. Therefore, the results obtained under this approximation can be easily applied to the photospheric level. On the other hand, coronal conditions require more sophisticated calculations.

We only consider a very simple configuration with homogeneous twist and uniform axial flow. It would be interesting to study the effect of a flow in more complicated configurations. Baty (2001) considered the triggering of kink instabilities in different magnetic field configurations and shows that each equilibrium has its particular threshold of instability, especially when the loop radius a is comparable to or less than the pitch p. We expect that longitudinal flows may reduce the instability threshold in any configuration, but probably with different mathematical expressions than those in Eqs. (23) or (28). This point can be subject of future study.

6. Conclusions

We have shown that the axial mass flow reduces the kink instability threshold in twisted magnetic tubes. Lundquist's stability criterion is replaced by the new formula

$$a > 2p\,(1 + kp)\,\sqrt{1 - M_A^2\,\rho_e/\rho_0},$$

where M_A is the Alfvénic Mach number. The influence of mass flow is more pronounced for photospheric tubes with $\rho_e/\rho_0 > 1$ than for coronal ones. However, a sufficiently high (but sub-Alfvénic) flow may trigger the kink instability in otherwise stable configurations of coronal loops and prominences, leading to the solar flares and CMEs. The phenomenon can be of importance for the solar photosphere/corona and space weather predictions.

For coronal conditions (and even more for prominence material), the stability thresholds are almost the same as the ones given by Dungey & Loughhead (1954) and Bennett et al. (1999) substituting their frequency by the Doppler-shifted frequency, since in these conditions $\rho_0 > \rho_e$, and since $\tilde{\omega} \approx kpM$, $\tilde{\omega}^2\rho_e/\rho_0 \ll P_m(ka)$ in Eq. (13), so the only non-Doppler-shifted frequency can be substituted by the Doppler-shifted one. Hence, the only effect is that an intense flow may unstabilize a very twisted configuration close to the instability margin, but otherwise the only contribution is to Doppler-shift the frequencies of the modes.

Finally, even a slight magnetic tube twist leads to the Kelvin-Helmholtz instability of axial sub-Alfvénic flows. The condition for the Kelvin-Helmholtz instability is

$$|m|M_A^2 > 1 + \rho_0/\rho_e.$$

Modes with sufficiently large m which yield nearly perpendicular propagation to the magnetic field (i.e. $m \approx -kp$) are always

unstable. Therefore any sub-Alfvénic flow quickly becomes unstable even in a slightly twisted tube if the longitudinal wavelength k multiplied by the pitch p is big enough.

Acknowledgements. The work of T.Z. was supported by the Austrian Fond zur Förderung der Wissenschaftlichen Forschung (project P21197-N16) and the Georgian National Science Foundation grant GNSF/ST09/4-310. A.J.D. thanks the Spanish MICINN for support under a Juan de la Cierva Postdoc Grant. A.J.D., R.O., and J.L.B. also acknowledge the financial support from the Spanish MICINN, FEDER funds, under Grant No. AYA2006-07637. T.Z. acknowledges the hospitality of the Departament de Física of the Universitat de les Illes Balears, where this work was done.

References

Archontis, V., Moreno-Insertis, F., Galsgaard, K., Hood, A., & O'Shea, E. 2004, A&A, 426, 1047
Baty H. 2001, A&A, 367, 321
Bennett, K., Roberts, B., & Narain, U. 1999, Sol. Phys., 185, 41
Brown, D. S., Nightingale, R. W., Alexander, D., et al. 2003, Sol. Phys., 216, 79
Browning, P. K., Gerrard, C., Hood, A. W., Kevis, R., & van der Linden, R. A. M. 2008, A&A, 485, 837
Carter, B. K., & Erdélyi, R. 2008, A&A, 481, 239
Chandrasekhar, S. 1961, Hydrodynamic and Hydromagnetic Stability (London: Oxford University Press)
Cirtain, J. W., et al. 2007, Science, 318, 1580
Cohn, H. 1983, ApJ, 269, 500
De Pontieu, B., et al. 2007, PASJ, 59, S655
Drazin, P. G., & Reid, W. H. 1981, Hydrodynamic Stability (Cambridge: Cambridge University Press)
Dungey, J. W., & Loughhead, R. E. 1954, Austr. J. Phys., 7, 5
Ferrari, A., Trussoni, E., & Zaninetti, L. 1981, MNRAS, 196, 1051
Furno, I., Intrator, T. P., Lapenta, G., et al. 2007, Phys. Plasmas, 14, 022103
Hood, A. W., & Priest, E. R. 1979, Sol. Phys., 64, 303
Hood, A. W., Archontis, V., Galsgaard, K., & Moreno-Insertis, F. 2009, A&A, 503, 999
Gerrard, C. L., Hood, A. W., & Brown, D. S. 2004, Sol. Phys., 222, 79
Goossens, M., Hollweg, J. V., & Sakurai, T. 1992, Sol. Phys., 138, 223
Gruszecki, M., Murawski, K., & Ofman, L. 2008, A&A, 488, 757
Katsukawa, Y., et al. 2007, Science, 318, 1594
Lin, Y., Engvold, O., & Wiik, J. E. 2003, Sol. Phys., 216, 109
Lin, Y., Engvold, O., Rouppe van der Voort, L. H. M., Wiik, J. E., & Berger, T. E. 2005, Sol. Phys., 226, 239
Linton, M. G., Dahlburg, R. B., Fisher, G. H., & Longcope, D. W. 1998, ApJ, 507, 404
Liu, R., Alexander, D., & Gilbert, H. R. 2007, ApJ, 661, 1260
Lundquist, S. 1951, Phys. Rev., 83, 307
Moreno-Insertis, F., & Emonet, T. 1996, ApJ, 472, L53
Murray, M. J., & Hood, A. W. 2008, A&A, 479, 567
Nishizuka, N., Shimizu, M., Nakamura, T., et al. 2008, ApJ, 683, L83
Ofman, L., & Wang, T. J. 2008, A&A, 482, L9
Okamoto, T. J., et al. 2007, Science, 318, 1557
Pataraya, A. D., & Zaqarashvili, T. V. 1995, Sol. Phys., 157, 31
Priest, E. R., Hood, A. W., & Anzer, U. 1989, ApJ, 344, 1010
Roberts, B. 1987, ApJ, 318, 590
Roberts, P. H. 1956, ApJ, 124, 430
Scullion, E., Popescu, M. D., Banerjee, D., Doyle, J. G., & Erdélyi, R. 2009, ApJ, 704, 1385
Sen, A. K. 1963, Phys. Fluids., 6, 1154
Singh, A. P., & Talwar, S. P. 1994, Sol. Phys., 149, 331
Shibata, K., et al. 1992, PASJ, 44, L177
Shibata, K., Nakamura, T., Matsumoto, T., et al. 2007, Science, 318, 1591
Soler, R., Oliver, R., & Ballester, J. L. 2008, ApJ, 684, 725
Soler, R., Oliver, R., & Ballester, J. L. 2009, ApJ, 693, 1601
Soler, R., Terradas, J., Oliver, R., Ballester, J. L., & Goossens, M. 2010, ApJ, 712, 875
Srivastava, A. K., Zaqarashvili, T. V., Kumar, P., & Khodachenko, M. L. 2010, ApJ, 715, 292
Terradas, J., Andries, J., Goossens, M., et al. 2008, ApJ, 687, L115
Terradas, J., Goossens, M., & Ballai, I. 2010, A&A, 515, A46
Terra-Homem, M., Erdélyi, R., & Ballai, I. 2003, Sol. Phys., 217, 199
Velli, M., Hood, A. W., & Einaudi, G. 1990, ApJ, 350, 428
Vasheghani Farahani, S., Van Doorsselaere, T., Verwichte, E., & Nakariakov, V. M. 2009, 498, L29
Winebarger, A. R., Warren, H., van Ballegooijen, A., DeLuca, E. E., & Golub, L. 2002, ApJ, 567, L89
Yan, X. L., & Qu, Z. Q. 2007, A&A, 468, 1083
Zhou, G. P., Wang, J. X., Zhang, J., et al. 2006, ApJ, 651, 1238